Dynamic eye model for adaptive optics testing

Enrique J. Fernández* and Pablo Artal

Laboratorio de Óptica, Departamento de Física, Centro de Investigación en Óptica y Nanofísica, Universidad de Murcia, Campus de Espinardo, 30071 Murcia, Spain

*Corresponding author: enriquej@um.es

Received 16 January 2007; revised 11 May 2007; accepted 6 July 2007;
posted 16 July 2007 (Doc. ID 79069); published 26 September 2007

An artificial dynamic eye model is proposed. The prototype enabled us to introduce temporal variations in defocus and spherical aberration, resembling those typically found in the human eye. The eye model consisted of a meniscus lens together with a modal liquid crystal lens with controllable focus. A diffuser placed at a fixed distance from the lenses acted as the artificial retina. Developed software allowed the user to precisely control the dynamic generation of aberrations. In addition, different refractive errors could simultaneously be emulated by varying the distance between the components of the model. The artificial eye was first used as a dynamic generator of both spherical aberration and defocus, imitating the behavior of a real eye. The artificial eye was implemented in an adaptive optics system designed for the human eye. The system incorporated an electrostatic deformable mirror and a Hartmann–Shack wavefront sensor. Results with and without real time closed-loop aberration correction were obtained. The use of the dynamic artificial eye could be quite useful for testing and evaluating adaptive optics instruments for ophthalmic applications.

OCIS codes: 010.1080, 330.4460, 220.4830.

1. Introduction

Adaptive optics (AO) allows the measurement and subsequent correction of optical aberrations. The technique is particularly suited to those situations where aberrations change over time. This is the case occurring in the human eye, where the aberrations present temporal fluctuations in the range of a few hertz [1]. In recent years, AO has been successfully applied for the study of the human eye [2,3]. The technique provides what could be a unique method for understanding the impact and effect of aberrations in vision [4–10]. Another important application of AO is ophthalmoscopy. The combination of this technique with the different imaging modalities, such as flood illumination fundus cameras [11], scanning laser ophthalmoscopes [12–14], and optical coherence tomography [15–19], has notably increased the achievable resolution of retinal images, enabling the *in vivo* investigation of morphological structures, otherwise hidden in conventional retinal imaging.

Ideally, AO for the eye should provide a high retinal image quality stable over time, eliminating the dynamic variations. The first dynamic process of importance in the optics of the human eye is accommodation [20], which is the ability of the eye to focus on the retina images of objects placed at different distances. The temporal response of the human eye in accommodation depends on a wide number of factors, such as the age of the subject, the movement of the object, the light level, etc. Even when the eye is accommodated at a steady distance, or even under cyclopegia (with the accommodation paralyzed) induced by drugs, there are temporal variations of the focus in the form of microfluctuations [20]. Fluctuations in such other aberration terms as coma, astigmatism, or spherical aberration are also present in the human eye. However, their amplitudes are weaker than those observed for defocus [1].

There is no equivalent to the useful Fried parameter or the Kolmogorov statistics [21], widely used in astronomical optics, to model the dynamic behavior of ocular aberrations. Perhaps a function to characterize the temporal changes of the eye's optics was never achieved, because of the inherent biological nature of the system. When designing optical systems to be

0003-6935/07/286971-07$15.00/0

applied to the human eye, in particular for AO systems, the absence of a theoretical model for the dynamics of the ocular aberration makes computational simulations useless. Even in the early stages of the design, the employment of real subjects is mandatory in AO, rendering the testing of such apparatus long and complicated. The development of those AO systems has to be based on the researcher's experience in many cases.

In this context, we propose in this paper an artificial dynamic eye model, resembling the temporal and spatial characteristics of the aberrations typically found in normal human eyes, to avoid, or alleviate, some of the previously reported problems when building ocular AO instruments.

2. Methods

A. Artificial Dynamic Eye

The elements of the artificial dynamic eye (ADE) were a liquid crystal lens, a linear polarizer, a positive lens, and a diffuser. The eye model is depicted in Fig. 1. The part of the ADE responsible for the static aberrations consisted of a positive lens, a meniscus lens of high power (~40 D), together with the diffuser. The diffuser was a rugose plastic piece coupled to a rotating motorized stage, allowing for different angular velocities. The rotation of the diffuser was performed in the direction normal to the incoming light, whose spatial coherence could be effectively broken, depending on the degree of coherence of the incident light, the angular velocity of the diffuser, and the detection specifications. The plastic plate mimed the human retina. The diffuser, together with the rotating stage, was mounted on a movable platform manually controlled by a micrometric screw. This design enabled the distance between the meniscus and the diffuser to be accurately changed, allowing the user to induce the desired amount of fixed defocus.

The dynamic part of the artificial eye was a liquid crystal (LC) lens (manufactured by Okotech [22]), together with a linear polarizer. Both elements were set in the ADE before the meniscus lens, as Fig. 1 shows. The temporal variations were introduced in the system by means of the LC lens.

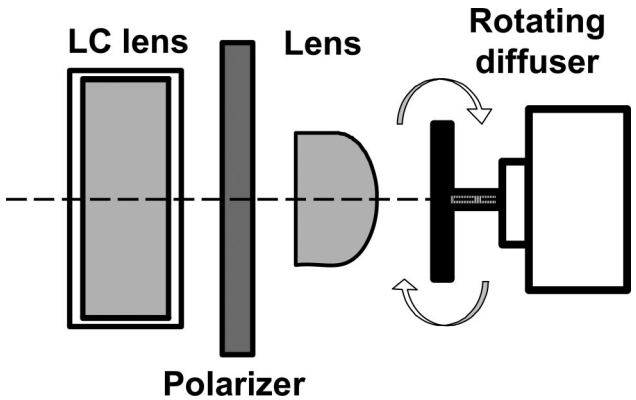

Fig. 1. Artificial dynamic eye components. The liquid crystal lens and the polarizer introduce dynamic changes in the eye. The meniscus lens of huge power concentrates light onto a rotating diffuser, acting as an artificial retina.

LC lenses are devices whose application in AO presents several advantages: low control voltages, transmission operation, and simplicity in the control [23,24]. The LC lens is essentially composed of a layer of nematic crystal surrounded by a transparent electrode. The nematic crystal presents birefringence characteristics, showing the capability to align its molecules in response to relatively weak electrical fields, causing its power consumption to be very low [25]. The electrode embracing the nematic crystal produces changes in the electrical field, which rotates the direction of the molecules in the LC. This yields a continuous variation of the refractive index of the crystal that is translated into phase variation over the incident beam. It produces light passing through the crystal that can be focused at different distances depending on the electrical signal applied to the electrode. Due to its low power consumption, the LC lens can be controlled from a personal computer by means of a control card with no need of other external power supply sources. The LC lens solely works over the component of the light parallel to the initial direction of the nematic molecules, consequently making mandatory the use of linear polarized light. That was the reason to place the polarizer in the ADE. The operating range of the LC lens in the ADE ranged from 1 to 0.25 D when using its maximum aperture (5 mm diameter). Transmittance was around 70% for wavelengths from 630 to 850 nm.

The artificial eye was modeled by using geometrical optics for simplicity. It was interesting to study the effective defocus of the entire system, so that refractive errors could be induced during the experiments in a controlled manner. Essentially, the eye was compounded by two positive lenses. The lens corresponding to the LC presented variable power, which had to be taken into account. The total defocus of the system was obtained as a function of the focal distances f' of both the meniscus and the LC lenses:

$$Defocus = -\frac{z}{\left(\frac{f_M' f_{LC}'}{e - f_M' - f_{LC}'}\right)^2}. \quad (1)$$

Index M refers to the meniscus lens, responsible for most of the power in the ADE. LC corresponds to the variable lens made of nematic crystal. The distance between the two lenses is given by e. The parameter z was obtained from

$$z = d - \left(\frac{f_M e}{(e - f_M') - f_{LC}'} + \frac{f_M' f_{LC}'}{e - f_M' - f_{LC}'}\right), \quad (2)$$

where d is the distance between the meniscus lens and the rotating diffuser.

Equation (1) shows that controlling the final range of variation of defocus as well as its central value was

possible by adjusting the distances d and e. This characteristic made the eye model versatile and useful to simulate different accommodative states and refractive errors.

It has to be said that in the preceding calculations both lenses were taken as thin ones. The mathematical expressions were derived assuming that the principal planes of the lenses were coincident for each lens [26]. In the case of the meniscus lens, due to its thickness and power, this assumption could be rough in some cases. The simplification is valid when other distances involved in the calculations, particularly d and e, are larger than the thickness of the meniscus lens. That was always our case in this paper. Even when d and e are comparable with the thickness of the meniscus, the inclusion of the different positions of the two principal planes did not yield a significant improvement in the accuracy of the obtained values, although the complexity of the mathematical expressions describing the final defocus notably increased.

A computer program was developed to control the ADE. The routines were written in C programming language. The program controlled the LC lens, permitting the user to produce random focal distances within a selected range, between 1 and 0.25 D. The statistical distribution of the generated focal distances followed a Gaussian function centered at the mean value of the interval, whose width could be selected in the program. The focal distances sequence, a pseudorandom sequence [27], was started by a seed number manually introduced in the program. The frequency of variation of the pseudorandom focal distances sequence was also a parameter to be fixed before every run. The described operation of the program, where frequency, range, and seed number for the automatic generation of focal distances were to be set by the user, enabled those pseudorandom sequences to be exactly repeated at any time.

B. Adaptive Optics System

The ADE was implemented in an AO system. The system was essentially similar to that designed for the measurement and correction in real time of the ocular aberrations described elsewhere [2]. Figure 2 shows a schematic of the AO system. The experimental apparatus incorporated an electrostatic deformable mirror [22] to compensate for the aberrations. The correcting device was endowed with 37 independent electrodes underneath the flexible membrane. The performance and technical characteristics of the deformable mirror have been studied in previous works [28]. In the system, two telescopes of different magnification conjugated the exit pupil of the ADE into the plane of the deformable mirror (L1 and L2, focal lengths of 120 and 200 mm, respectively), and on the wavefront sensor plane (L3 and L4, focal lengths of 200 and 100 mm, respectively). Total magnification of the system was 0.83. Aberrations were measured by a Hartmann–Shack sensor [29]. The latter was formed by an array of square microlenses, 0.6 mm width and 6.3 mm focal length. A video CCD camera at 25 Hz obtained the images from the sensor,

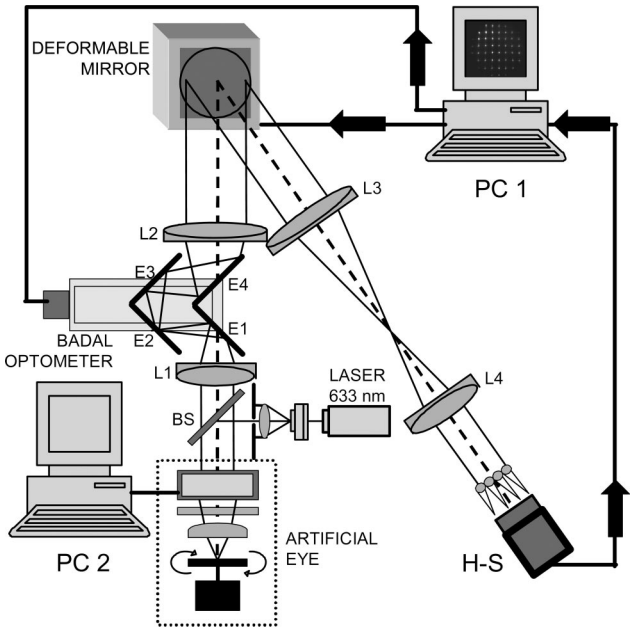

Fig. 2. Adaptive optics system for the human eye to test the capabilities of the artificial dynamic eye. System incorporates a Hartmann–Shack wavefront sensor and an electrostatic deformable mirror for measuring and correcting the aberrations, respectively.

to be processed in a computer at video rate. Appropriate software used those measurements to control in real time the shape of the deformable mirror in a closed loop, so that aberrations could be compensated in real time [28]. The AO system also incorporated a Badal optometer (mirrors E1, E2, E3, and E4) mounted on a motorized stage to control defocus independently in the apparatus. This part of the system has shown notable advantages when working with amounts defocus out of the range of correction of the deformable mirror. A He–Ne laser emitting at 632.8 nm illuminated the ADE after reflection in an uncoated pellicle beam splitter (~90% transmission), as Fig. 2 shows. The principle of operation of the whole system was similar to the standard procedure widely employed for the human eye [29,30]: a narrow beam from the He–Ne laser source of 1 mm diameter was introduced in the eye model. Light incident in the rotating diffuser was backscattered, passing through the ADE. The wavefront at the exit of the LC lens was measured by the Hartmann–Shack sensor.

3. Results

The capabilities of the ADE to produce changes in defocus were first tested in the AO system. The deformable mirror was inactive during these measurements, presenting a near plane surface (peak-valley $< \lambda/4$). Pupil size was limited to 3.2 mm diameter. The effect of introducing different seed numbers in the control program was evaluated. Figure 3 shows the fluctuations in defocus occurring for several series of pseudorandom sequences, as they were retrieved by the Hartmann–Shack wavefront sensor during 5 s.

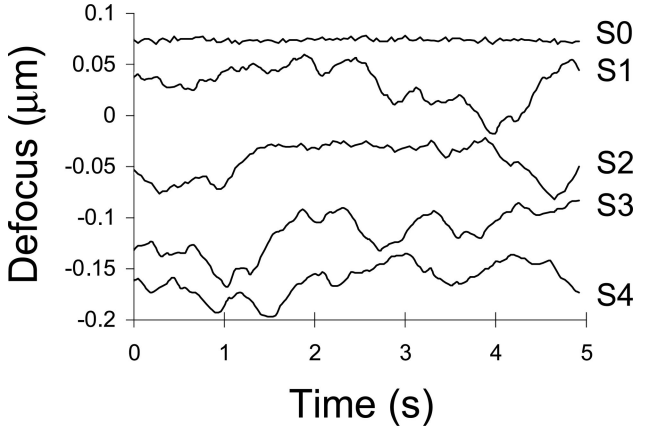

Fig. 3. Effect of using different seed numbers for the generation of pseudorandom series of defocus fluctuations in the artificial dynamic eye. S0 corresponds to the noise of the system.

Defocus is described in the figure as the coefficient of the fourth Zernike polynomial in the Optical Society of America ordering [31], and it is given in micrometers. S0 corresponds to the case of no defocus induction, providing a measurement of the existing noise during the runs, also assuring that changes were strictly produced by the LC lens and no other artifacts were involved. The noise arises from the frame-to-frame variation in the estimation of the wavefront. Consequently, it exhibits a maximum at 25 Hz. For the presented measurements, the programmed frequency of variation was 8.33 Hz, allowing the LC lens to operate within its maximum range: from 1 to 0.25 D. The resulting mean standard deviation of the four series was 0.018 μm. Defocus was shifted in the ADE for a better visualization of the sequences of fluctuations.

The ADE, by the effect of using the LC lens, introduced in the system not only dynamic changes in defocus, but also in other aberrations. The second term of importance in absolute magnitude was the spherical aberration. This particular aberration appears because of the nonlinear response of the nematic crystal near the edges of the transparent case containing the LC. To obtain short focal distances it is necessary to use the whole range of phase variation. The spherical aberration is present due to the saturation produced in the border of the crystal. Other aberrations, such as coma aberration and astigmatism, might also be present due to small defects in the width of the nematic layer, but their contribution is rather weak as compared to that of defocus or even spherical aberration [25].

The performance of the ADE emulating the behavior of ocular aberrations found in the human eye, in particular when reproducing defocus and spherical aberration fluctuations, was tested in the system.

Ocular aberrations were obtained in the system from a real eye, subject of 40 years old with no ocular conditions, through a pupil of 4.7 mm diameter [29]. Most of the refractive error of the eye, 1.25 D myopic, was precompensated by means of the motorized

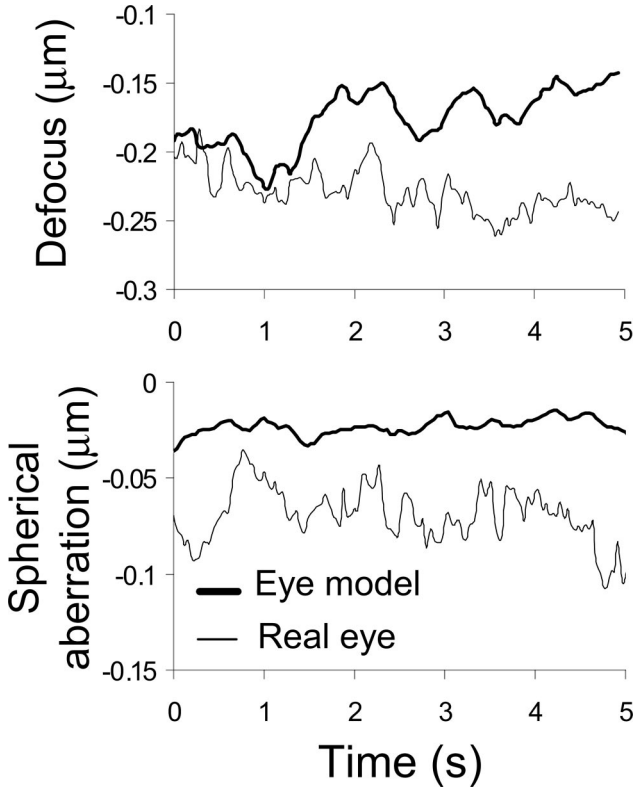

Fig. 4. Comparison of defocus and spherical aberration dynamics generated by the artificial dynamic eye and those measured from a real eye.

Badal optometer. Parameters of the artificial eye were afterward set to emulate the evolution of defocus obtained from the real eye, using the same pupil size. The distance between the two lenses of the ADE, e, and between the diffuser and the meniscus lens, d, were 0.08 ± 0.01 and 0.025 ± 0.01 m, respectively. Programmed frequency of variation was similar to the case presented in Fig. 3, 8.33 Hz, from 1 to 0.25 D.

Figure 4 shows the comparison between both defocus and spherical aberration obtained from the ADE and those measured in the real eye. The strength of the fluctuations in defocus for the real and the artificial eye were relatively similar in this case, as the standard deviations in both cases showed: 0.021 and 0.025 μm, respectively. The initial level of defocus was also set in the ADE to mimic that from the real eye. Maintaining the values of the parameters in the ADE, spherical aberration generated by the eye model was also studied. In this case, the ADE produced a standard deviation and a mean value different than those measured from the real eye. Figure 5 shows the average power spectra for both defocus and spherical aberration. The dark curve corresponds to the results obtained from the ADE, while the other depicts those from the real eye. For the spherical aberration, the relative strength of the frequencies in the spectra was conserved, making the curves near parallel. They did not overlap as in the case of defocus, where the absolute weight of certain frequencies was similar for the artificial and the real eye.

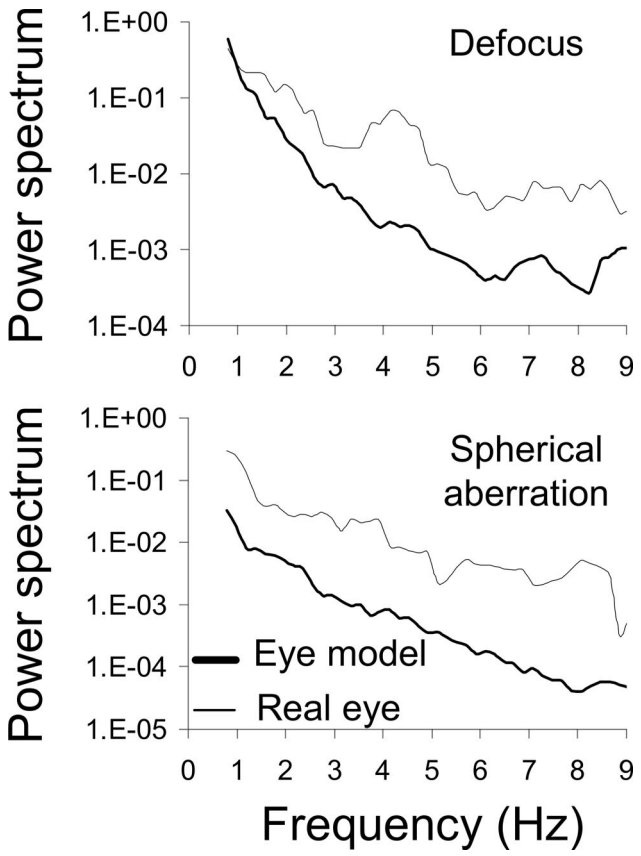

Fig. 5. Power spectrum of defocus and spherical aberration dynamics generated by the artificial dynamic eye and those measured from a real eye.

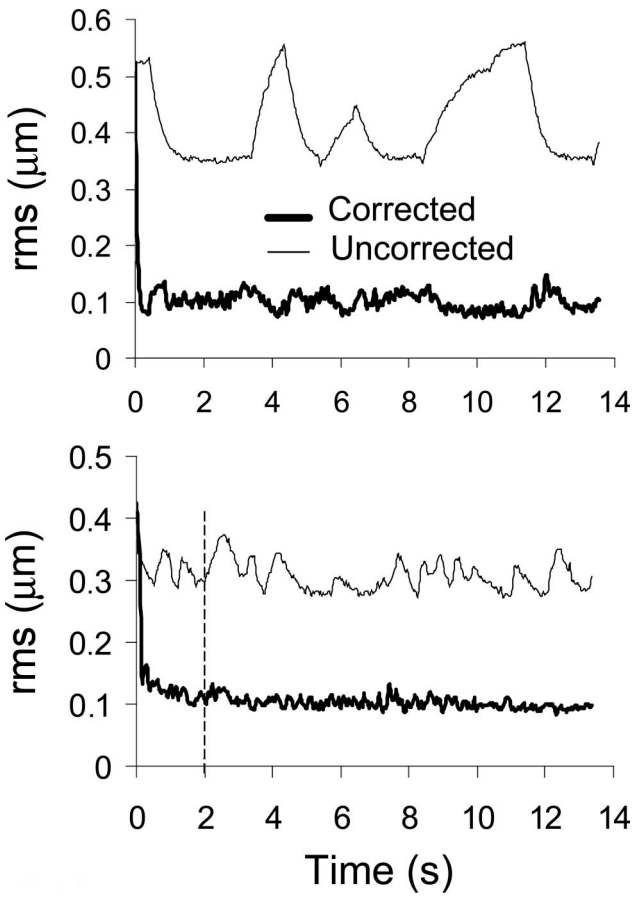

Fig. 6. Closed-loop aberration correction of the artificial dynamic eye by the AO system under different dynamic conditions.

The ADE was used for AO testing. In particular, the capabilities of the AO system for measuring and correcting aberrations were investigated with the eye model. Figure 6 shows two examples of aberration correction corresponding to two different sets of parameters programmed in the ADE. The figure shows the evolution of the total root-mean-square (rms) of the measured wavefront as a function of time along 14 s through a pupil of 4.6 mm diameter. The light curve shows the evolution of the rms with no aberration correction, while the dark curve corresponds to the case with closed-loop AO aberration correction. It must be noted that the same seed number was used for each graphic to start the pseudorandom sequence of focal variation in the control program, keeping identical experimental conditions in both cases: corrected and uncorrected. Consequently, identical evolution of the rms, except for a small factor introduced by noise, from the ADE was obtained in both cases, allowing direct comparison between curves. On top, the frequency of variation in the ADE was fixed at 1 Hz within the maximum range of variation. The figure at the bottom depicts the results when the ADE was programmed to generate defocus variations with a frequency of 3 Hz, again within its maximum range, introducing a mean defocus of -0.43 μm. In this particular case, the ADE was also set to introduce higher-order aberrations. Those aberrations can be statically induced in the system by simply misaligning and decentering the meniscus lens in the ADE. Due to its large power, even small tilts caused a noticeable amount of astigmatism and other aberrations. Figure 7 provides quantitative information of the aberrations of the ADE for this last case. Black bars present the values of the Zernike coefficients

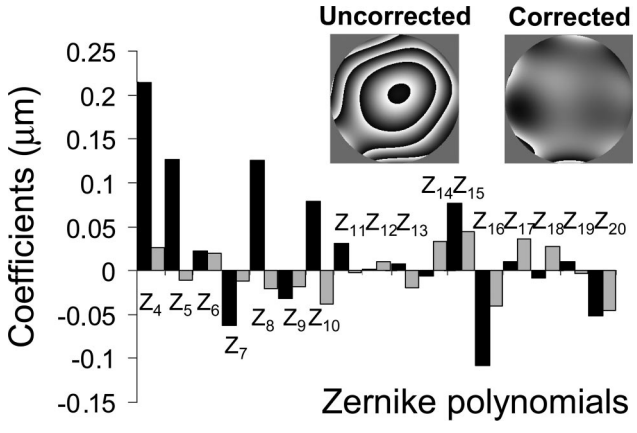

Fig. 7. Zernike coefficients with and without aberration correction (gray and black color, respectively) from the artificial dynamic eye. Corresponding wavefronts are shown with modulus 2π representation at 633 nm.

with no correction after 2 s, while gray bars indicate aberrations during AO correction, at the same time. Tilts and piston terms have not been included in the figure. Astigmatism and coma aberration (Z5 and Z8, respectively) are present. Even higher-order terms as those corresponding to Z15 and Z16 arise in the figure. A modulus 2π representation of the wavefront has been included in the figure for the corrected and uncorrected case, providing qualitative information about the AO correction.

4. Conclusions

Different human eyes present different dynamic responses. Consequently, a useful dynamic eye model must permit an easy adjustment, within the adequate ranges, of the values of the variables whose evolution is to be simulated. The proposed ADE has demonstrated its ability to mimic different states of accommodation in a controlled manner. Fluctuations around the central value in both defocus and spherical aberration, with different amplitudes and frequencies, were possible to be set in the control program. Higher-order aberrations, with increased prevalence in the pathologic and elderly eye although also occurring in the normal eye, can be induced in the model by tilting and decentering the meniscus lens.

It must be noticed that the production of defocus and spherical aberration with the artificial eye cannot resemble simultaneously those typically found in real eyes. The source of the mismatch between the production of defocus and spherical aberration can be easily understood from the different mechanisms inducing them. In the case of the artificial eye, defocus is obtained from the profile of refractive index induced in the liquid crystal by the electric field applied to the transparent electrode surrounding the material. The strength of the field decreases to the square of the distance, so the shape of the wavefront passing through the entire surface of the liquid crystal resembles a sphere (defocus), making the beam converge. When the range of possible electric field rotating the molecules of the liquid crystal is surpassed, the relation between electric field and refractive index is no longer linear, appearing in this case as a spherical aberration. The latter occurs as a consequence of the different radius of curvature of the wavefront from the center to the periphery. Given that spherical aberration arises in those situations where the electric field takes values above a certain threshold, its frequency cannot be the same as the one obtained for defocus.

Nevertheless, the artificial eye could be programmed to produce spherical aberration with a given frequency upon previous calibration. This is a significant difference in the dynamics of the artificial eye compared to the case of a real eye, which might be taken into account when implementing the model. In the real eye, the main source of variation for defocus and spherical aberration is the fluctuation of the crystalline lens, whose power continuously changes within small ranges. As a result of this variation, the temporal evolution of these two aberrations is similar, contrary to the case of the ADE.

The same AO system has been used for measuring both a real eye and the ADE, with no need of previous adaptation or calibration, showing the eye model to be easy to implement in those complex systems.

Direct comparison between the corrected and uncorrected wavefront is for the first time possible by using the ADE. This can be simply accomplished by using the same seed number in the generation of sequences of variation of defocus, therefore assuring an identical evolution of the wavefront. The use of the ADE for testing AO systems, specifically those developed to operate with the human eye, can notably help to identify problems, limitations, or artifacts sometimes arising in closed-loop systems, making the design procedure more effective.

A possible alternative method to characterize an AO system consists in forcing the closed loop up to its maximum temporal limit. The artificial eye that we have used in combination with the adaptive optics setup in the present work does not permit that. The reason is twofold: the liquid crystal implemented in the artificial eye exhibits a moderate dynamic range of nearly 10 Hz of variation with noticeable amplitude; and the AO is designed to correct aberrations above 10 Hz. Nevertheless, the design and the idea we proposed can be implemented using other types of faster state-of-the-art liquid crystal with a higher temporal dynamic, being in this case possible to evaluate up to their limit adaptive optics systems exhibiting fast temporal operation.

Due to the temporal response of the liquid crystal implemented in the proposed artificial eye, the changes to be emulated correspond mainly to those appearing as a consequence of the fluctuations in accommodation [32], and associated with the cardiopulmonary system [33]. However, other variations presenting higher frequencies are known to affect the optical quality of the retinal image, related to instabilities and changes occurring at the tear film covering the cornea [34,35]. For these latter phenomena, the presented artificial eye is unable to show a comparable dynamic range.

Other improvements could benefit the ADE for certain applications. Recently, the simultaneous correction of monochromatic and chromatic aberrations [36], referred to as pancorrection [37] has been demonstrated with potential benefit in optical coherence tomography [18]. Lenses introducing amounts of chromatic aberration similar to those typically found in the human eye can be used in the ADE, making the model also useful under polychromatic illumination.

This research was supported by the Ministerio de Educacion y Ciencia, Spain (grant FIS2004-02153).

References

1. H. Hofer, P. Artal, B. Singer, J. L. Aragón, and D. R. Williams, "Dynamics of the eye's wave aberration," J. Opt. Soc. Am. A **18,** 497–506 (2001).

2. E. J. Fernández, I. Iglesias, and P. Artal, "Closed-loop adaptive optics in the human eye," Opt. Lett. **26,** 746–748 (2001).
3. H. Hofer, L. Chen, G. Y. Yoon, B. Singer, Y. Yamauchi, and D. R. Williams, "Improvement in retinal image quality with dynamic correction of the eye's aberrations," Opt. Express **8,** 631–643 (2001).
4. E. J. Fernández, S. Manzanera, P. Piers, and P. Artal, "Adaptive optics visual simulator," J. Refract. Surg. **18,** 634–638 (2002).
5. P. Artal, L. Chen, E. J. Fernández, B. Singer, S. Manzanera, and D. R. Williams, "Neural compensation for the eye's optical aberrations," J. Vision **4,** 281–287 (2004).
6. E. J. Fernández and P. Artal, "Study on the effects of monochromatic aberrations in the accommodation response by using adaptive optics," J. Opt. Soc. Am. A **22,** 1732–1738 (2005).
7. P. Piers, E. J. Fernández, S. Manzanera, S. Norrby, and P. Artal, "Adaptive optics simulation of intraocular lenses with modified spherical aberration," Invest. Ophthalmol. Vis. Sci. **45,** 4601–4610 (2004).
8. L. Chen, P. B. Kruger, H. Hofer, B. Singer, and D. R. Williams, "Accommodation with higher-order monochromatic aberrations corrected with adaptive optics," J. Opt. Soc. Am. A **23,** 1–8 (2006).
9. K. M. Hampson, C. Paterson, C. Dainty, and E. A. H. Mallen, "Adaptive optics system for investigation of the effect of the aberration dynamics of the human eye on steady-state accommodation control," J. Opt. Soc. Am. A **23,** 1082–1088 (2006).
10. B. J. Wilson, K. E. Decker, and A. Roorda, "Monochromatic aberrations provide an odd-error cue to focus direction," J. Opt. Soc. Am A **19,** 833–839 (2002).
11. J. Rha, R. S. Jonnal, K. E. Thorn, J. Qu, Y. Zhang, and D. T. Miller, "Adaptive optics flood-illumination camera for high speed retinal imaging," Opt. Express **14,** 4552–4569 (2006).
12. A. W. Dreher, J. F. Bille, and R. N. Weinreb, "Active optical depth resolution improvement of the laser tomographic scanner," Appl. Opt. **28,** 804–808 (1989).
13. A. Roorda, F. Romero–Borja, W. J. Donnelly III, H. Queener, T. J. Hebert, and M. C. W. Campbell, "Adaptive optics scanning laser ophthalmoscopy," Opt. Express **10,** 405–412 (2002).
14. Y. Zhang, S. Poonja, and A. Roorda, "MEMS-based adaptive optics scanning laser ophthalmoscopy," Opt. Lett. **31,** 1268–1270 (2006).
15. B. Hermann, E. J. Fernández, A. Unterhuber, H. Sattmann, A. F. Fercher, W. Drexler, P. M. Prieto, and P. Artal, "Adaptive optics ultrahigh resolution optical coherence tomography," Opt. Lett. **29,** 2142–2144 (2004).
16. Y. Zhang, J. Rha, R. S. Jonnal, and D. T. Miller, "Adaptive optics spectral optical coherence tomography for imaging the living retina," Opt. Express **13,** 4792–4811 (2005).
17. R. Zawadzki, S. Jones, S. Olivier, M. Zhao, B. Bower, J. Izatt, S. Choi, S. Laut, and J. Werner, "Adaptive-optics optical coherence tomography for high-resolution and high-speed 3D retinal in vivo imaging," Opt. Express **13,** 8532–8546 (2005).
18. E. J. Fernández, B. Považay, B. Hermann, A. Unterhuber, H. Sattmann, P. M. Prieto, R. Leitgeb, P. Ahnelt, P. Artal, and W. Drexler, "Three-dimensional adaptive optics ultrahigh-resolution optical coherence tomography using a liquid crystal spatial light modulator," Vision Res. **45,** 3432–3444 (2005).
19. Y. Zhang, B. Cense, J. Rha, R. S. Jonnal, W. Gao, R. J. Zawadzki, J. S. Werner, S. Jones, S. Olivier, and D. T. Miller, "High-speed volumetric imaging of cone photoreceptors with adaptive optics spectral-domain optical coherence tomography," Opt. Express **14,** 4380–4394 (2006).
20. K. F. Ciuffreda, "Vision and visual dysfunction," in *Accommodation and Its Anomalies,* J. Cronly–Dillon, ed. (J. R. Macmillan Press, 1991), Chap. 11.
21. R. K. Tyson, *Principles of Adaptive Optics,* 2nd ed. (Academic, 1997).
22. http://www.okotech.com.
23. A. F. Naumov, G. D. Love, M. Y. Loktev, and F. L. Vladimirov, "Control optimization of spherical modal liquid crystal lenses," Opt. Express **4,** 344–352 (1999).
24. A. F. Naumov, M. Y. Loktev, I. R. Guralnik, and G. Vdovin, "Liquid-crystal adaptive lenses with modal control," Opt. Lett. **23,** 992–994 (1998).
25. M. Y. Loktev, V. N. Belopukhov, F. L. Vladimirov, G. V. Vdovin, G. D. Love, and A. F. Naumov, "Wavefront control systems based on modal liquid crystal lenses," Rev. Sci. Instrum. **71,** 3290–3297 (2000).
26. W. H. Press, S. A. Teukolsky, W. T. Vetterling, and B. P. Flannery, *Numerical Recipes in C,* 2nd ed. (Cambridge U. Press, 1992).
27. M. Born and E. Wolf, *Principles of Optics,* 6th ed. (Pergamon, 1987).
28. E. J. Fernández and P. Artal, "Membrane deformable mirror for adaptive optics: performance limits in visual optics," Opt. Express **11,** 1056–1069 (2003).
29. P. M. Prieto, F. Vargas–Martín, S. Goelz, and P. Artal, "Analysis of the performance of the Hartmann–Shack sensor in the human eye," J. Opt. Soc. Am. A **17,** 1388–1398 (2000).
30. J. Liang, B. Grimm, S. Goelz, and J. F. Bille, "Objective measurement of wave aberrations of the human eye with use of a Hartmann–Shack wavefront sensor," J. Opt. Soc. Am. A **11,** 1949–1955 (1994).
31. L. N. Thibos, R. A. Applegate, J. T. Schwiegerling, R. H. Webb, and V. S. T. Members, "Standards for reporting the optical aberrations of eyes," in *Vision Science and Its Applications,* Vol. 35 of OSA Trends in Optics and Photonics (Optical Society of America, 2000), pp. 110–130.
32. W. N. Charman, "Fluctuations in accommodation: a review," Ophthalmic Physiol. Opt. **8,** 153–163 (1988).
33. K. M. Hampson, I. Munro, C. Paterson, and C. Dainty, "Weak correlation between the aberration dynamics of the human eye and the cardiopulmonary system," J. Opt. Soc. Am. A **22,** 1241–1250 (2005).
34. S. Gruppetta, F. Lacombe, and P. Puget, "Study of the dynamic aberrations of the human tear film," Opt. Express **13,** 7631–7636 (2005).
35. K. Y. Li and G. Yoon, "Changes in aberrations and retinal image quality due to tear film dynamics," Opt. Express **14,** 12552–12559 (2006).
36. E. J. Fernández, A. Unterhuber, B. Považay, B. Hermann, P. Artal, and W. Drexler, "Chromatic aberration correction of the human eye for retinal imaging in the near infrared," Opt. Express **14,** 6213–6225 (2006).
37. E. J. Fernández, L. Vabre, B. Hermann, A. Unterhuber, B. Považay, and W. Drexler, "Adaptive optics with a magnetic deformable mirror: applications in the human eye," Opt. Express **14,** 8900–8917 (2006).